

''

## Simulations of pulsatile blood flow in tapered S-shaped in-plane and out-of-plane coronary arteries

Barbara M. Johnston and Peter R. Johnston

*School of Biomolecular and Physical Sciences, Griffith University, Nathan, Queensland  
E-mail: P.Johnston@griffith.edu.au*

**Abstract:** Ischaemic heart disease has been the leading cause of death in Australia for the past 10 years. Included in this category are angina, blocked arteries and heart attacks. This paper presents a modelling study of the precursors to artery blockage, namely coronary artery disease, or narrowing of the coronary arteries, based on geometrical considerations.

It is believed that wall shear stress is a key initiating factor in coronary artery disease, especially low wall shear stress. Wall shear stress is caused by the blood flowing along the walls of the artery and in regions of low wall shear stress the flow is relatively slow compared to that in other parts of the artery. In these slow flow regions, there is enhanced opportunity for molecules carried in the blood (for example low density lipoproteins (LDL)) to diffuse out of the blood and into the artery wall. Long term exposure to this diffusive process results in thickening of the artery wall and, hence, narrowing of the available area for blood flow within the artery. Of major concern are regions of the coronary arteries which demonstrate consistently low wall shear stress over the cardiac cycle.

The complex flow patterns observed in coronary arteries are believed to be related to the pulsatile nature of the flow, the rheological properties of the blood and the geometry of the arteries, including branching, bifurcation and curvature. Possible factors that may cause differences in the coronaries compared with other arteries in the body are the particular character of the coronary inlet velocity waveform and the fact that coronary velocities are lower than most of the other arteries, which, with their smaller diameters, leads to lower Reynolds numbers. Other factors may be their tortuous nature, which includes out-of-plane bends.

The combination of the complicated three dimensional structure of the coronary arteries and the complex flow patterns makes it difficult to isolate factors affecting wall shear stress (WSS) distributions along the artery walls. Here, as a way to simplify the complications, we present a series of transient simulations to model blood flow in tapered, three-dimensional, in-plane and out-of-plane, S-shaped coronary arteries. The simulations are performed by solving the three dimensional Navier-Stokes and continuity equations which govern fluid flow. It is also assumed that blood behaves as an incompressible Newtonian fluid.

In each of the arteries, for the majority of the cycle (that is, during forward flow), "high" WSS is found on the outside of each bend and (relative to this) "low" WSS on the inside of the bend. Within each of these low stress regions a point of consistently low WSS (that is, low throughout the entire cardiac cycle) can be identified. In addition, the tapered arteries considered here also show a region of consistently low WSS in the proximal region of the artery, where the majority of plaques are found in the coronary arteries. Such points are not observed in constant radius artery models. In every case these points of consistently low WSS appear to be related to the planar geometry of the artery only and not to the form of the inlet waveform used or whether the curvature is in-plane or out-of-plane.

The identification of a region of consistently low wall shear stress in the straight inlet (proximal) region in the model with tapered arteries (and not in the model with constant radius arteries) fits with postmortem findings. It then follows that this region of low WSS in realistic coronary arteries is due, in part, to the overall taper in the artery and not only to the local curvature variation.

It is concluded that, to realistically model coronary arteries, it is necessary to include taper and also out-of-plane bends.

**Keywords:** *blood flow, taper, coronary arteries, computational fluid dynamics, out-of-plane bend, wall shear stress*

# 1 Introduction

It has long been recognised that atherosclerotic lesions develop preferentially at specific sites in certain arteries, such as the aortic arch, carotid bifurcation, infrarenal, femoral and coronary arteries. Clinical observations have found that plaques form predominantly on the inside of curves and the outer walls of vessel bifurcations (Asakura and Karino, 1990) and studies have shown that these sites co-localise with regions of low shear stress (Malek et al., 1999).

It is believed that wall shear stress is a key initiating factor in the development of these lesions Caro et al. (1971), especially low wall shear stress Nerem (1992). Wall shear stress is caused by the blood flowing along the walls of the artery and in regions of low wall shear stress the flow is relatively slow compared to that in other parts of the artery. In these slow flow regions, there is enhanced opportunity for molecules carried in the blood (for example low density lipoproteins (LDL)) to diffuse out of the blood and into the artery wall. Long term exposure to this diffusive process results in thickening of the artery wall and, hence, narrowing of the available area for blood flow within the artery. Of major concern are regions of the coronary arteries which demonstrate consistently low wall shear stress over the cardiac cycle.

There are many possible factors which can cause differences in the coronaries compared with other arteries in the body. These include the particular character of the coronary inlet velocity waveform and the fact that coronary velocities are lower than most of the other arteries mentioned above, which, with their smaller diameters, leads to lower Reynolds numbers. Other factors may be their tortuous nature, including out-of-plane bends Caro et al. (1996).

In the case of the coronary arteries, experimental studies on human right coronary arteries obtained at autopsy (Ojha et al., 2001) have found that the proximal region of the right coronary artery (RCA) appears to be a site of intrinsic eccentric intimal thickening, with maximum thickness on the myocardial side of the artery and that this is not the case in other regions. Another study (Wang et al., 2004) analysed 208 patients with ST-segment elevation myocardial infarctions and mapped the location of the acute coronary occlusion, finding that occlusions tended to cluster in the proximal third of each of the coronary vessels studied (RCA, left anterior descending (LAD) and left circumflex artery (LCX)). Further studies of other arteries within the body indicate that there are differences, between coronary arteries and the arteries mentioned above, which influence the formation of plaque in the proximal region.

There have been various studies which model blood flow in the coronary arteries, using a range of assumptions. Some examples of three-dimensional transient studies are: RCAs with uniform cross-section (Zeng et al., 2003); anatomically realistic RCAs (Johnston et al., 2006); slightly curved tube (LCA section) (Perktold et al., 1991) and idealised U-shaped curved section (Jung et al., 2006). In addition, Chen *et al.* (Chen and Lu, 2006) conducted a modelling study in a bifurcation model containing a non-planar branch, with an inlet diameter of 8mm (much larger than coronary artery diameter dimensions of around 3-5mm). An earlier modelling study of steady flow in an S-curve, simulating part of a femoral artery, was conducted by Hoogstraten *et al.* (Hoogstraten et al., 1996). Also, Qiao *et al.* (Qiao et al., 2004) considered pulsatile flow in two in-plane constant radius S-shaped curves with 6 mm and 3 mm radii, in order to numerically simulate blood flow in the aorta and minor arteries. In these latter two cases, however, the inlet velocity waveform used was a flow rate waveform of an ascending aorta, with a maximum velocity of 1.4 m/s over a 0.4 second cycle, which corresponds to a pulse-rate of 150 beats per minute. We have previously considered flow in in-plane and out-of-plane S-shaped models with uniform diameter at a more realistic 60 beats per minute (Johnston and Johnston, 2008).

Since realistic coronary arteries have complex geometrical structures, the work in this paper is an attempt to consider what effect factors such as the character of the inlet velocity waveform and geometrical features such as arterial curvature and tapering may have on blood flow in simplified coronary arteries. The aim is to use realistic coronary velocities (less than 0.5 m/s (Perktold et al., 1991)) and consider the flow in an S-shaped artery, to simplify the number of bends and changes in curvature being considered. Also, a consistent feature of coronary arteries is that they taper from the proximal to the distal ends (Johnston et al., 2004). The first S-shaped 'coronary' artery considered here is similar to the first artery of Qiao *et al.* (Qiao et al., 2004), except that the artery tapers; the second artery is the same as the first except that it contains an out-of-plane bend. In each case the simulations are performed using both a left coronary artery (LCA) (Perktold et al., 1991) and a RCA (Matsuo et al., 1988) waveform, so that the effect of the two different inlet velocity waveforms can be studied, as well as comparing the in- and out-of-plane arteries. Blood flow within the arteries will be compared in terms of axial and secondary velocities, wall shear stress (WSS) and oscillatory shear index (OSI).

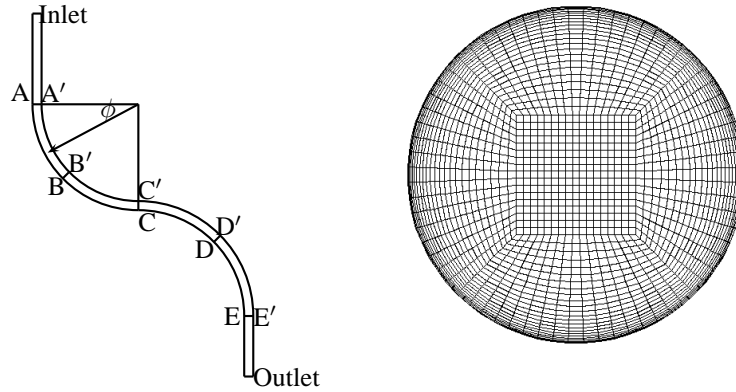


Figure 1: The tapered in-plane S-shaped artery (not to scale) (left) and the inlet mesh for all arteries (right).

## 2 Methods

### 2.1 Geometry

This work considers simulations of blood flow in two different rigid, circular cross-section, S-shaped arteries: (a) **s2d**: an evenly tapering in-plane S-shaped artery, shown in Fig. 1 (without taper), with an outlet radius of 78% of the inlet radius; and (b) **s3d**: the same artery as in (a), except that the second bend, beginning at  $CC'$ , is normal to the plane of the first, resulting in the outlet being parallel to the plane of the page in Fig. 1. For both arteries, the straight inlet and outlet sections are 3 cm and 2 cm long, respectively, and the radius of curvature  $R_c$  of the curved sections is 3.5 cm, giving an overall artery length of 16 cm, similar to realistic arteries considered previously (Johnston et al., 2004). The inlet radius  $R$  for both arteries is 2 mm, while the outlet radius is 1.56 mm.

### 2.2 Mathematical Model

In these simulations blood is represented by an incompressible Newtonian fluid, governed by the continuity and conservation of momentum equations:

$$\nabla \cdot \underline{v} = 0 \quad \text{and} \quad \rho \underline{v} \cdot \nabla \underline{v} = \mu \nabla^2 \underline{v} - \nabla P \quad (1)$$

where  $\underline{v}$  is the 3D velocity vector,  $P$  pressure,  $\rho$  density ( $1056 \text{ kg m}^{-3}$ ) and  $\mu$  viscosity ( $0.00345 \text{ Pa s}$ ). These equations are solved subject to the following boundary conditions: (a) on the walls, a no-slip condition is imposed on the velocities; (b) at the outlet, tangential stresses and gauge pressure are set to zero; (c) at the inlet, a uniform velocity profile is used, with a time varying forcing function having a period,  $T$ , of one second (60 beats per minute), representative of either a left (Fig. 2(a) (Perktold et al., 1991)) or a right (Fig. 2(b) (Matsuo et al., 1988)) coronary artery flow waveform.

Characteristic parameters for these simulations can then be calculated using the following definitions (Qiao et al.,

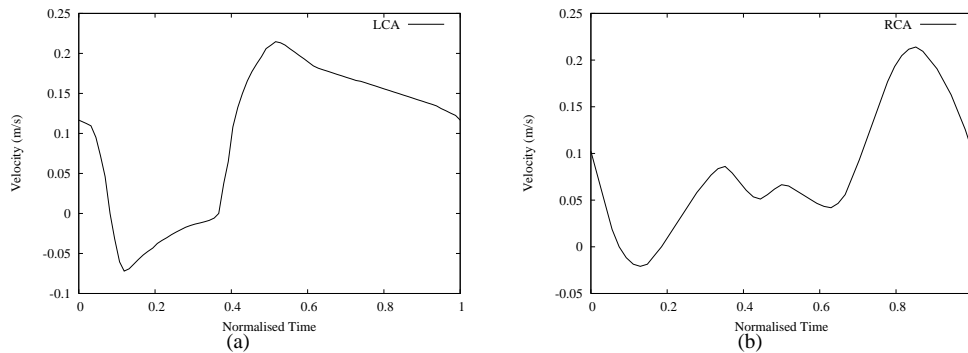


Figure 2: (a) Left coronary artery (Perktold et al., 1991) and (b) right coronary artery (Matsuo et al., 1988) inlet velocity waveforms.

2004) for maximum Reynolds number  $Re$ , Womersley number  $\alpha$  and Dean number  $Dn$ :

$$Re = \frac{2Rv_{max}\rho}{\mu}, \quad \alpha = \sqrt{\frac{2\pi\rho}{T\mu}}R, \quad Dn = Re\sqrt{\delta}, \quad \text{where } \delta = R/R_c \quad (2)$$

This gives  $Re = 226$ ,  $\alpha = 2.6$ ,  $Dn = 54$  and  $\delta = 0.057$  at the inlet of both s2d and s3d. The coronary artery parameters used here are similar to those used previously (Jung et al., 2006) and to other studies quoted therein.

Equations (1), subject to the above boundary conditions, are solved on the grid of Section 2.4, with the finite volume method, using the commercially available software package CFD-ACE (CFDRC, Huntsville, Alabama, USA) for performing the computational fluid dynamics simulations. The model is run over about five cycles to ensure the solutions at the start and end of the cycle are identical, since the simulations represent a temporally cyclic phenomenon.

### 2.3 Definitions

The various simulations are compared in terms of parameters such as wall shear stress  $\tau_w$  and oscillatory shear index OSI (He and Ku, 1996), which are defined as

$$\tau_w = -\mu \left. \frac{\partial v}{\partial n} \right|_{\text{wall}} \quad \text{and} \quad \text{OSI} = \frac{1}{2} \left[ 1 - \frac{\left| \int_0^T \tau_w dt \right|}{\int_0^T |\tau_w| dt} \right] \quad (3)$$

These parameters are compared at various points or sections on the artery, as shown in Fig. 1, where sections AA', BB', CC', DD' and EE' correspond to  $\phi$  values of  $0^\circ$ ,  $45^\circ$ ,  $90^\circ$ ,  $135^\circ$  and  $180^\circ$ , respectively.

### 2.4 Computational Grid

The s2d and s3d meshes used in this work are constructed using the GEOM package available in CFD-ACE (CFDRC, Huntsville, Alabama, USA) and each consists of 192 882 nodes with the inlet mesh shown in Fig. 1. Mesh independence is established by performing additional simulations with increased numbers of nodes in the radial direction. As the simulations presented here are transient, values of the OSI are used in comparisons. On a refined mesh it is found that the OSI differs from that on the original mesh by less than 0.1%. Hence the original mesh is considered sufficiently accurate to be used for the following simulations.

## 3 Results

### 3.1 Wall Shear Stress and its Extremes

The pattern of WSS in s3d LCA is shown in Fig. 3(a) at  $t=0.52$ . ‘‘High’’ WSS can be seen on the outside of curves and, relative to this, ‘‘low’’ WSS on the inside of curves. Superimposed on this is an increase in WSS between the proximal and the distal ends of the artery. WSS is found to be qualitatively similar to this for the majority of the forward flow phase of cardiac cycle, for both the in-plane and out-of-plane arteries, and both input waveforms. The pattern is reversed during back flow, so that high WSS is now on the inside of the curve and low WSS on the outside.

Although the pattern of WSS is qualitatively the same at different times during forward flow, the magnitude of WSS varies with time, according to the applied velocity waveform. This can be seen in s3d LCA by the similarity between Fig. 4, which shows WSS throughout the cardiac cycle at the points X, C' and E (see Fig. 3 for the location of the points), and the LCA forcing function shown in Fig. 2(a).

After considering WSS throughout the entire cardiac cycle, three points, X, C' and E, are identified as having the consistently lowest maximum values of WSS, denoted  $\min(\max WSS)$ , with the global minimum at X. These points are observed in all four in-plane and out-of-plane LCA and RCA arteries. This can be seen in Table 1, which lists each of these points and various values, such as time and value of  $\min(\max WSS)$ , at each of the points. These results would appear to indicate that neither the inlet velocity waveform nor the presence or absence of out-of-plane bends affects the position of these points of consistently low WSS throughout the cardiac cycle and that they are simply related to the planar geometry of the artery. These observations are valid for all four artery models considered.

It is the case, however, that the introduction of a taper does affect the magnitude of WSS, which is found to increase as the radius decreases down the artery. A consequence of this is that the point of global  $\min(\max WSS)$  moves from C' for the uniform radius arteries (Johnston and Johnston, 2008) up the artery to X (Fig. 3) for the tapered arteries. This is a very interesting result because it suggests that points of low WSS are likely to be found in the proximal region of the coronary arteries, where the radius is large and more or less constant, a region where plaque develops preferentially in coronary arteries (Ojha et al., 2001; Wang et al., 2004).

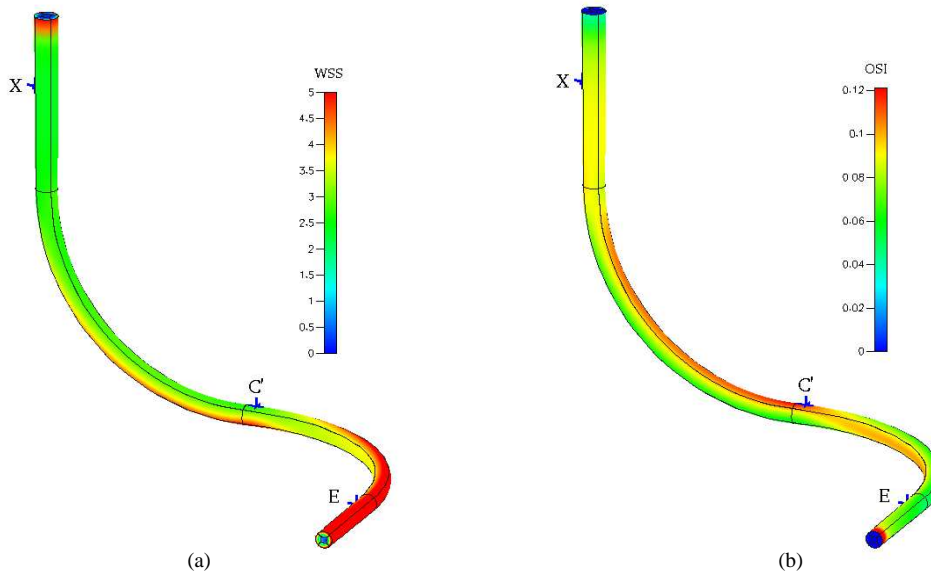


Figure 3: (a) Wall Shear Stress at  $t=0.52$  and (b) OSI, in s3d LCA.

Artery	Position of $\min(\max WSS)$	Time of $\min(\max WSS)$	Value of $\min(\max WSS)$	OSI at $\min(\max WSS)$
LCA s2d	X	0.49	2.39	0.09
LCA s3d	X	0.49	2.39	0.09
LCA s2d	C'	0.49	2.52	0.13
LCA s3d	C'	0.49	2.65	0.12
LCA s2d	E	0.49	3.31	0.12
LCA s3d	E	0.49	3.32	0.12
RCA s2d	X	0.84	2.36	0.04
RCA s3d	X	0.84	2.36	0.04
RCA s2d	C'	0.81	2.43	0.06
RCA s3d	C'	0.81	2.56	0.06
RCA s2d	E	0.82	3.22	0.05
RCA s3d	E	0.82	3.23	0.05

Table 1: The lowest maximum Wall Shear Stress at a point, over the cycle,  $\min(\max WSS)$ , and the point and time at which it occurs in the various simulations, as well OSI at that point. The table also presents the same data for the next two lowest maximums. The points X, C', and E are shown in Fig. 3.

### 3.2 Oscillatory Shear Index

From the definition given in Section 2.3, it can be seen that OSI is calculated as an average over the cardiac cycle to give a measure of the oscillatory nature of the flow at a point and that it takes on values in the range 0 to 0.5. So it is possible to consider OSI at each point throughout the artery and find points with high OSI values, which would indicate more oscillatory flow at those points than at others.

A plot of OSI in s3d LCA is presented in Fig. 3(b) and, when this is compared with WSS in the same artery in Fig. 3(a), it is apparent that, apart from the straight inlet region, locally “low” WSS and “high” OSI seem to be correlated, allowing for the fact that WSS increases from the proximal to the distal ends of the artery.

OSI values for the four arteries are calculated at the points X, C' and E and the values are included in Table 1. In general, these values of OSI are very near to maximum values, for that particular simulation. From Table 1, it can be seen that within either the LCA or the RCA, “low” values of WSS correspond to “high” values of OSI, as discussed above, except at the point X, where WSS is lowest, but OSI is only moderate there. It can also be seen that OSI in the LCA is higher than in the RCA. Since the axial velocity profile is symmetric at X and there are no eddies there, the only contribution to the OSI value comes from the changes in flow due to the inlet velocity waveform. This would explain the low value of OSI at X compared with that at C'.

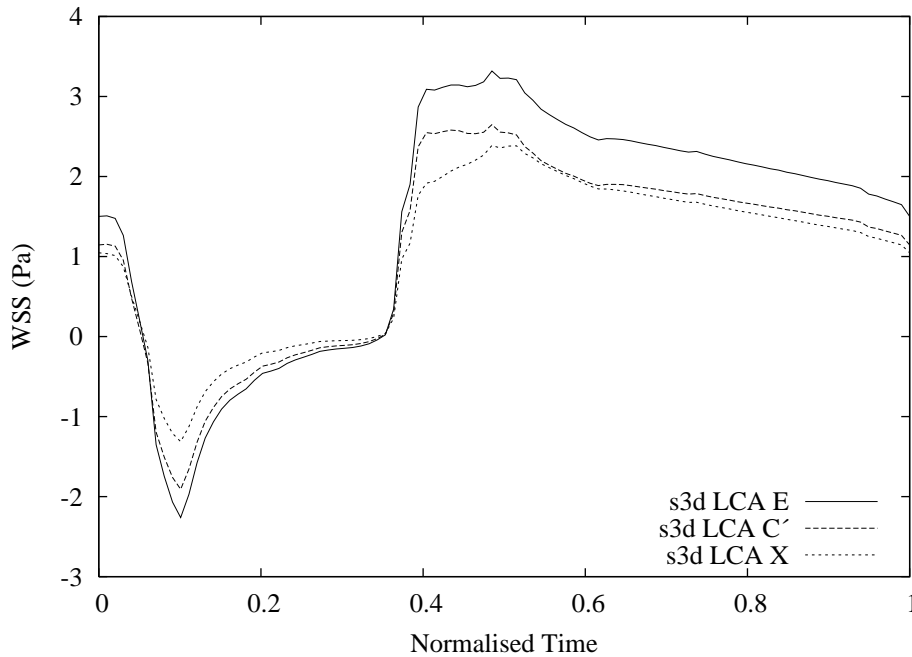


Figure 4: Wall Shear Stress in s3d LCA at X, C' and E. See Fig. 3 for locations of points.

## 4 Discussion and Conclusions

This study considers flow in simplified, but tapering, coronary arteries. However, realistic flow waveforms for right and left coronary arteries are used. Despite these apparent simplifications, the results of this study agree with findings from previous experimental studies.

The fact that WSS at any point on the artery varies in time according to the inlet velocity waveform has been noted by Jung *et al.* (Jung *et al.*, 2006), who studied pulsatile flow in an idealised U-shaped section of a coronary artery (RCA) during resting conditions ( $v_{max} = 0.17$  m/s), using a two-phase viscosity method. They found lower than average WSS on the inside curve than the outside curve and this is in agreement with the results here as well as a number of other studies (Qui and Tarbell, 2000; Zeng *et al.*, 2003; Perktold *et al.*, 1991; Myers *et al.*, 2001). The study in a planar S-shaped artery with a constant radius, by Qiao *et al.* (Qiao *et al.*, 2004), which motivated the present study, also found high OSI values at C' and E. In addition, the increase in WSS between the proximal and distal ends of tapered arteries has been found in a simulation of the human LCA tree (Soulis *et al.*, 2006) and by the present authors as a general trend in several human RCAs (Johnston *et al.*, 2006). The fact that different inlet velocity waveforms have very little effect on the WSS patterns observed and that OSI values are very small, agrees with the findings of Myers *et al.* (Myers *et al.*, 2001) in their study using an anatomically realistic RCA.

Previous studies (Johnston *et al.*, 2006) in anatomically realistic RCAs have also identified proximal regions in the artery with consistently low WSS. The complex three dimensional geometric nature of the arteries makes it difficult to discern if the low WSS arises due to local curvature variation or perhaps because of overall tapering of the arteries. This study, with its simplified geometry and taper, identifies a region of low WSS in the straight inlet section of the model. It then follows that the region of low WSS in realistic arteries (Johnston *et al.*, 2006) is due partially to the overall taper in the artery and not only to the local curvature variation.

Points of consistently low WSS are also found at C' and E in identical constant radius (non-tapered) arteries (Johnston and Johnston, 2008). However, in the case of the tapered arteries, an additional point X (see Fig. 3) is found in the proximal region of the artery and this point is where the global minimum, of maximum WSS over the cycle, is located and this is the case for all of the tapered arteries studied. This leads to the conclusion that WSS patterns and points of consistently low WSS are determined entirely by the planar geometry of the artery. It is also consistent with the observed pattern of increased plaque in the proximal region of the coronary arteries, while in the narrower distal regions where few lesions are found, higher WSS acts in a preventative manner.

It seems, therefore, that the inlet velocity waveform chosen in modelling studies for coronary arteries is not crucial, but that tapering should definitely be used in such studies. The inclusion of out-of-plane bends, while not essential for studying patterns of WSS, is required to study realistic blood flow in the coronary arteries. Given that real coronary

arteries not only taper but also include sudden expansions and multiple changes in curvature (Johnston et al., 2006; Asakura and Karino, 1990), further work in this area could incorporate these features.

## References

- Asakura, T. and Karino, T. (1990). Flow patterns and spatial distribution of atherosclerotic lesions in human coronary arteries. *Circ. Res.*, 66:1045–1066.
- Caro, C. G., Doorley, D. J., Tarnawski, M., Scott, K. T., Long, Q., and Dumoulin, C. L. (1996). Non-planar curvature and branching of arteries and non-planar-type flow. *Proc. R. Soc. Lond. A*, 452:185–197.
- Caro, C. G., Fitz-Gerald, J. M., and Schroter, R. C. (1971). Atheroma and arterial wall shear: observation, correlation and proposal of a shear dependent mass transfer mechanism for atherogenesis. *Proc. R. Soc. Lond.*, B177:109–159.
- Chen, J. and Lu, X.-Y. (2006). Numerical investigation of the non-newtonian pulsatile blood flow in a bifurcation model with a non-planar branch. *Journal of Biomechanics*, 39(5):818–832.
- He, X. and Ku, D. N. (1996). Pulsatile flow in the human left coronary artery bifurcation: average conditions. *Transactions of the ASME*, 118:74–82.
- Hoogstraten, H. W., Kootstra, J. G., Hillen, B., Krijger, J. K. B., and Wensing, P. J. W. (1996). Numerical simulation of blood flow in an artery with two successive bends. *Journal of Biomechanics*, 29:1075–1083.
- Johnston, B. M., Johnston, P. R., Corney, S., and Kilpatrick, D. (2004). Non-Newtonian blood flow in human right coronary arteries: Steady state simulations. *Journal of Biomechanics*, 37(5):709–720.
- Johnston, B. M., Johnston, P. R., Corney, S., and Kilpatrick, D. (2006). Non-Newtonian blood flow in human right coronary arteries: Transient simulations. *Journal of Biomechanics*, 39(6):1116–1128.
- Johnston, P. R. and Johnston, B. M. (2008). Blood flow in S-shaped in-plane and out-of-plane coronary arteries. In Mercer, G. N. and Roberts, A. J., editors, *Proceedings of the 8th Biennial Engineering Mathematics and Applications Conference, EMAC-2007*, volume 49 of *ANZIAM J.*, pages C341–C358.
- Jung, J., Lyczkowski, R. W., Panchal, C. B., and Hassanein, A. (2006). Multiphase hemodynamic simulation of pulsatile flow in a coronary artery. *Journal of Biomechanics*, 39(11):2064–2073.
- Malek, A. M., Seth, L. A., and Izumo, S. (1999). Hemodynamic shear stress and its role in atherosclerosis. *JAMA*, 282(21):2035–2042.
- Matsuo, S., Tsuruta, M., Hayano, M., Immamura, Y., Eguchi, Y., Tokushima, T., and Tsuji, S. (1988). Phasic coronary artery flow velocity determined by Doppler flowmeter catheter in aortic stenosis and aortic regurgitation. *The American Journal of Cardiology*, 62(1):917–922.
- Myers, J. G., Moore, J. A., Ojha, M., Johnston, K. W., and Ethier, C. R. (2001). Factors influencing blood flow patterns in the human right coronary artery. *Annals of Biomedical Engineering*, 29:109–120.
- Nerem, R. M. (1992). Vascular fluid mechanics, the arterial wall, and atherosclerosis. *ASME J. Biomedical Engng*, 114:274–282.
- Ojha, M., Leask, R. L., Butany, J., and Johnston, K. W. (2001). Distribution of intimal and medial thickening in the human right coronary artery: a study of 17 RCAs. *Atherosclerosis*, 158:147–153.
- Perktold, K., Nerem, R. M., and Peter, R. O. (1991). A numerical calculation of flow in a curved tube model of the left main coronary artery. *J. Biomechanics*, 24(3–4):175–189.
- Qiao, A. K., Guo, X. L., Wu, S. G., Zeng, Y. J., and Xu, X. H. (2004). Numerical study of nonlinear pulsatile flow in S-shaped curved arteries. *Medical Engineering and Physics*, 26:545–552.
- Qui, Y. and Tarbell, J. M. (2000). Numerical simulation of pulsatile flow in a compliant curved tube model of a coronary artery. *Journal of Biomechanical Engineering*, 122:77–85.
- Soulis, J. V., Farmakis, T. M., Giannoglou, G. D., and Louridas, G. E. (2006). Wall shear stress in normal left coronary artery tree. *Journal of Biomechanics*, 39(4):742–749.
- Wang, J. C., Normand, S.-L. T., Mauri, L., and Kuntz, R. E. (2004). Coronary artery spatial distribution of acute myocardial infarction occlusions. *Circulation*, 110:278–284.
- Zeng, D., Ding, Z., Friedman, M. H., and Ethier, C. R. (2003). Effects of cardiac motion on right coronary artery hemodynamics. *Annals of Biomedical Engineering*, 31:420–429.